Journal of Alloys and Compounds 509 (2011) L169–L173

Contents lists available at ScienceDirect

Journal of Alloys and Compounds

journal homepage: www.elsevier.com/locate/jallcom

Letter

Spray formed Al-based amorphous matrix nanocomposite plate

Longchao Zhuo[a], Bin Yang[b], Hui Wang[a], Tao Zhang[a,*]

[a] Key Laboratory of Aerospace Materials and Performance (Ministry of Education), Department of Materials Science and Engineering, Beihang University, Beijing 100191, China
[b] State Key Laboratory for Advanced Metals and Materials. University of Science and Technology Beijing, Beijing 100083, China

ARTICLE INFO

Article history:
Received 1 December 2010
Received in revised form 21 February 2011
Accepted 22 February 2011
Available online 1 March 2011

Keywords:
Metallic glasses
Rapid-solidification
Microstructure
Mechanical properties

ABSTRACT

A novel $Al_{86}Si_{0.5}Ni_{4.06}Co_{2.94}Y_6La_{0.5}$ amorphous matrix nanocomposite plate with a rough diameter of 200 mm and a maximum thickness of 12 mm has been prepared by spray-forming. The microstructure gradient is observed, with 91.7 vol.% amorphous phase for the bottom region, 78% for the middle, and 54.3% for the top. The nanoindentation tests reveal its high microhardness of ~420 HV. The microstructure characterization indicates that the improved mechanical properties may be attributed to the homogeneously dispersed nano-scale fcc-Al in the amorphous matrix. This work further proved the feasibility of achieving substantial fraction of amorphous phase for bulk Al-based alloys by spray forming.

1. Introduction

Since Al-based amorphous ribbons were firstly reported in 1980s [1,2], the superior mechanical properties including high fracture tensile strength and 180° bending ductility have attracted much interest and led to abundant research on Al-based metallic glasses [3]. However, due to their limited glass-forming ability (GFA), the formation of Al-based metallic glasses or the amorphous matrix composites is still generally limited to the shape of thin ribbons, which obviously restricts their practical use [3,4]. Powder metallurgy has been employed to prepare bulk materials; however, this method suffers from porosity and contamination problems [5,6]. As a novel metallurgical process with the characteristics of rapid solidification, spray deposition [7–9] has been developed for the manufacture of near-net shape products, making possible atomization and consolidation in a single step. Therefore, a few recent attempts have been made to fabricate amorphous or nanocrystalline Al-based alloys by spray forming method. Afonso et al. [10,11] reported that the $Al_{85}Ni_5Co_2Y_8$ billet processed using high ratio of volumetric gas flow rate to mass of metal flow rate led to more fractions of featureless areas. Ted Guo et al. [12,13] observed featureless particles embedded in a crystalline matrix by spray forming the $Al_{89}Ni_5La_6$ and $Al_{85}Ni_{10}Nd_5$ alloys. Garcia-Escorial et al. [14] obtained a bulk $Al_{93}Fe_3Cr_2Ti_2$ alloy consisting of certain nanoquasicrystalline phase by spray forming. Strivastava et al. [15] reproduced the $Al_{85}Ni_5Co_2Y_8$ alloy by spray forming, resulted in a 12 mm thick composite plate including fcc-Al, Al_2Y, Al_3Y, and some unidentified phases, besides the formation of amorphous phase. Compared with the spray-formed Mg- [16] and La-based [17] monolithic bulk metallic glasses, the dominant constraint of spray forming Al-based bulk metallic glasses or nanocomposite still lies in the inherent limited GFA of the alloy former. More recently, Al-based alloys with relatively high GFA, for which the critical diameter for glass formation reaches or approaches 1 mm by copper mold casting, have been reported [18–20]. Therefore, in this paper, we choose the $Al_{86}Si_{0.5}Ni_{4.06}Co_{2.94}Y_6La_{0.5}$ alloy [19] as the spray former to study the feasibility of spray forming a bulk material with substantial amorphous phase. The microstructure, thermal properties as well as the mechanical properties of the spray-formed alloy are also studied.

2. Material and methods

The master alloy with nominal composition was prepared by arc melting pure metals (over 99.9 mass%) in argon atmosphere using a Ti-gettered arc-melter. Then the ingots with a total weight of 3 kg were remelted under argon atmosphere in a graphite crucible. The melt was kept for 15 min among 1200–1250 K to eliminate any un-melted alloying elements or high temperature compounds. Subsequently, the melt was poured into a pre-heated tundish and atomized with argon gas at a pressure of 0.6 MPa. The diameter of the nozzle bore of the atomizer, the flying distance and the ejection temperature are 3 mm, 600 mm, and 1100 K, respectively. The droplets were deposited onto a rotating steel substrate collector to form a rapid solidified preform. The alloy ribbons used for comparison were prepared by a single roller melt-spinning method in an argon atmosphere.

The spray-formed deposit was examined by X-ray diffraction (XRD) using a Bruker AXS D8 X-ray diffractometer with Cu-Kα radiation. Thermal analysis was performed on NETZSCH DSC 404 C differential scanning calorimeter (DSC) in a flowing purified argon atmosphere. The backscattered images of polished oversprayed

* Corresponding author. Tel.: +86 010 82339705; fax: +86 010 82334869.
E-mail address: zhangtao@buaa.edu.cn (T. Zhang).

0925-8388/$ – see front matter © 2011 Elsevier B.V. All rights reserved.
doi:10.1016/j.jallcom.2011.02.125

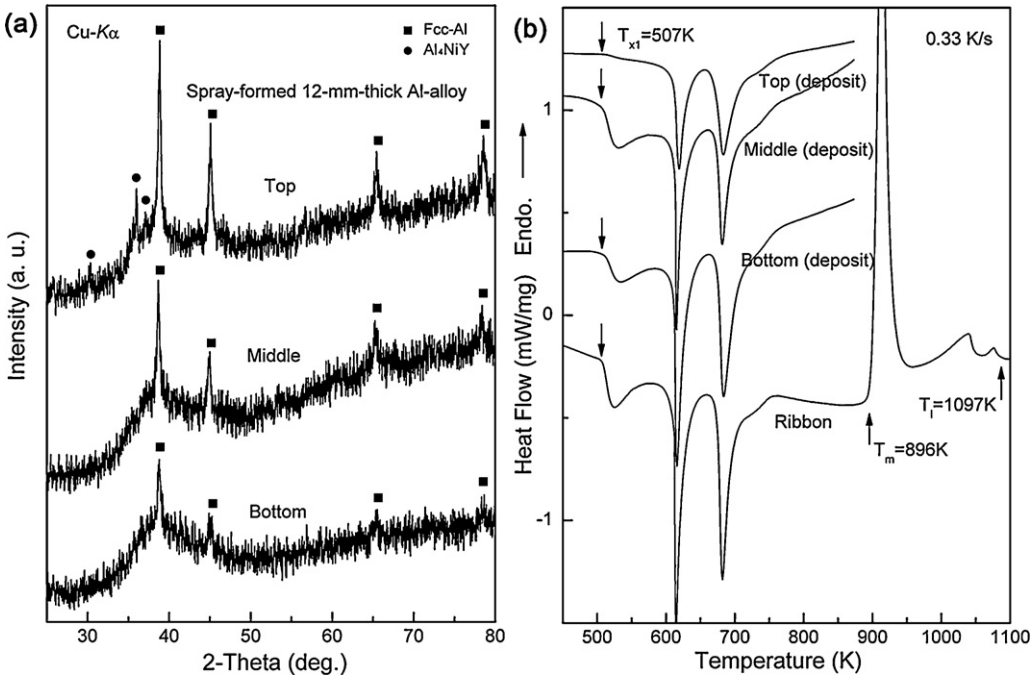

Fig. 1. (a) XRD patterns and (b) DSC traces taken from different regions of the spray-formed $Al_{86}Si_{0.5}Ni_{4.06}Co_{2.94}Y_6La_{0.5}$ deposit: top, middle and bottom.

powders and the deposit were obtained on JSM-5800 scanning electron microscopy (SEM) equipped with energy dispersive X-Ray spectroscopy (EDS). The structure of the deposit was also studied by JEOL 2100F high resolution transmission electron microscope (HRTEM). For TEM observation, the samples were mechanically ground to be ~80 μm thick and then electrochemically polished with a 25% nitric acid methanol solution at 243 K. Vickers microhardness was measured using 100 g indentation load applied for 10 s. Ten individual indents were tested on each sample. Depth-sensing indentation was conducted using a Nano Indenter II (MTS, US). Displacement (h) and loads (p) were measured with resolutions of 0.04 nm and 75 nN at 296 K, respectively.

3. Results and discussion

The spray-formed $Al_{86}Si_{0.5}Ni_{4.06}Co_{2.94}Y_6La_{0.5}$ deposit is an irregularly round plate with a rough diameter of 200 mm and a maximum thickness of 12 mm. Fig. 1(a) shows the XRD diffraction patterns of the representative samples taken from the maximum thickness, i.e. the center of the spray-formed deposit: the bottom region (1 mm perpendicularly away from the substrate), the middle region (5 mm perpendicularly away from the substrate), and the top region (11 mm perpendicularly away from the substrate). The amorphous phase covering a substantial volume fraction can be seen both for the bottom and middle region samples, with the patterns of fcc-Al superimposed on the broad maximum. While for the top region of the deposit, small traces of Al_4NiY, which might devitrified during the final spray forming process can be observed. The DSC curves of both spray-formed and melt-spun forms of the $Al_{86}Si_{0.5}Ni_{4.06}Co_{2.94}Y_6La_{0.5}$ alloy are shown in Fig. 1(b) for comparison. Both forms show well accordance with each other and exhibit three exothermic reactions. The total enthalpy released due to crystallization can be related with the volume fraction of the amorphous phase present [10–15,21]. The total crystallization energies of the ribbon and the top region of the deposit are approximately 119.58 J/g and 64.96 J/g, respectively. Therefore, using the 100% amorphous ribbon as the standard, the volume fraction of the amorphous phase for the top region of the deposit is about 54.3%. In the same method, the amorphous phases are calculated to be about 78 vol.% and 91.7 vol.%, respectively for the middle and the bottom regions of the deposit.

Backscattered images of oversprayed powders and the spray-formed deposit are shown in Fig. 2 to further study the microstructure. Fig. 2(a) shows spherical particles with different kinds of surface. The surface pattern can be related to the difference in the structure of the powders, i.e. smooth surface for amorphous and rough for crystalline [22]. The characteristic sphere is indicative of a high fraction of liquid droplets arrived on the substrate forming the deposit, avoiding the escape of the gas throughout the deposit. It is noticed that different microstructure features are often found in different powders, even from the similar size range. This difference is related to their different degree of undercooling and kinetic transitions experienced by droplets under different flight and solidification environments. Anyway, the critical diameter for the formation of the spherical amorphous phase can be estimated to be around 45 μm under the present experimental processing parameters. However, it should be noted that the solidification condition that the overspray powder experienced is different from that of the deposited droplets. In Fig. 2(b) for the axial cross section of the deposit, we observed considerable amount of pores with various shapes, which were formed by the solidification shrinkage and the gas entrapment during the solidification of the deposit [23]. Besides the pores, there is no distinct contrast revealing other micron-sized crystalline phase over the whole cross section, which indicates that the fcc-Al embedded in the amorphous matrix is in submicron or nanometer size, as shown in Fig. 2(c) and (d). However in the top region of the deposit, as indicated in Fig. 2(e) and (f), some precipitated micron-sized Al_4NiY as well as coarsened fcc-Al were observed according to the EDS analysis, which has also been checked in the corresponding TEM experiments.

Fig. 3(a) shows the bright field image with the selected area electron diffraction (SAED) pattern (the inset) taken from the middle region of the spray-formed $Al_{86}Si_{0.5}Ni_{4.06}Co_{2.94}Y_6La_{0.5}$ deposit. The electron diffraction patterns show the main broad amorphous ring plus diffraction peaks of fcc-Al. The nanocrystalline fcc-Al particles are homogeneously dispersed in the amorphous matrix and most of them are ranging from 20 to 50 nm. One fcc-Al crystallite particle surrounded by the amorphous matrix can be clearly seen from the high resolution electron image as shown in Fig. 3(b).

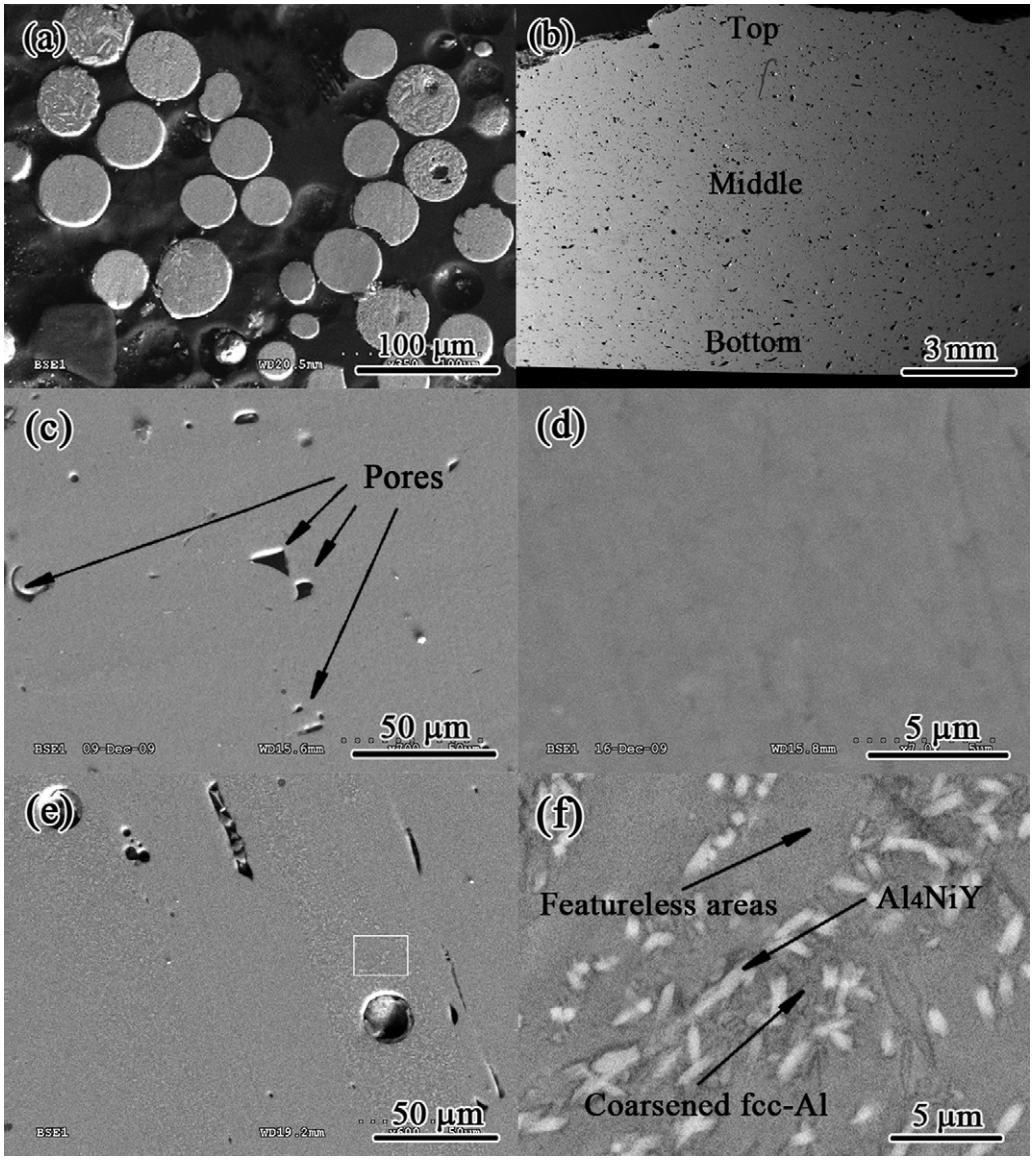

Fig. 2. Backscattered electron images of the polished samples: (a) oversprayed powders; (b) the axial cross section of the deposit; (c) and (d) representative images for the bottom and middle regions; and (e) and (f) the top region of the deposit. The rectangle indicated in (e) is enlarged as (f).

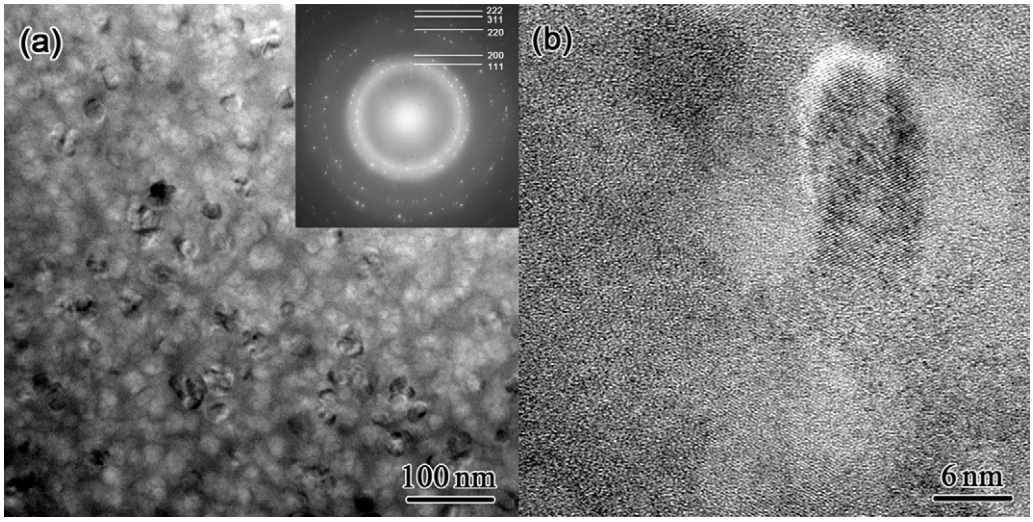

Fig. 3. (a) Bright field image with the SAED pattern inserted and (b) HRTEM image taken from the middle region of the spray-formed $Al_{86}Si_{0.5}Ni_{4.06}Co_{2.94}Y_6La_{0.5}$.

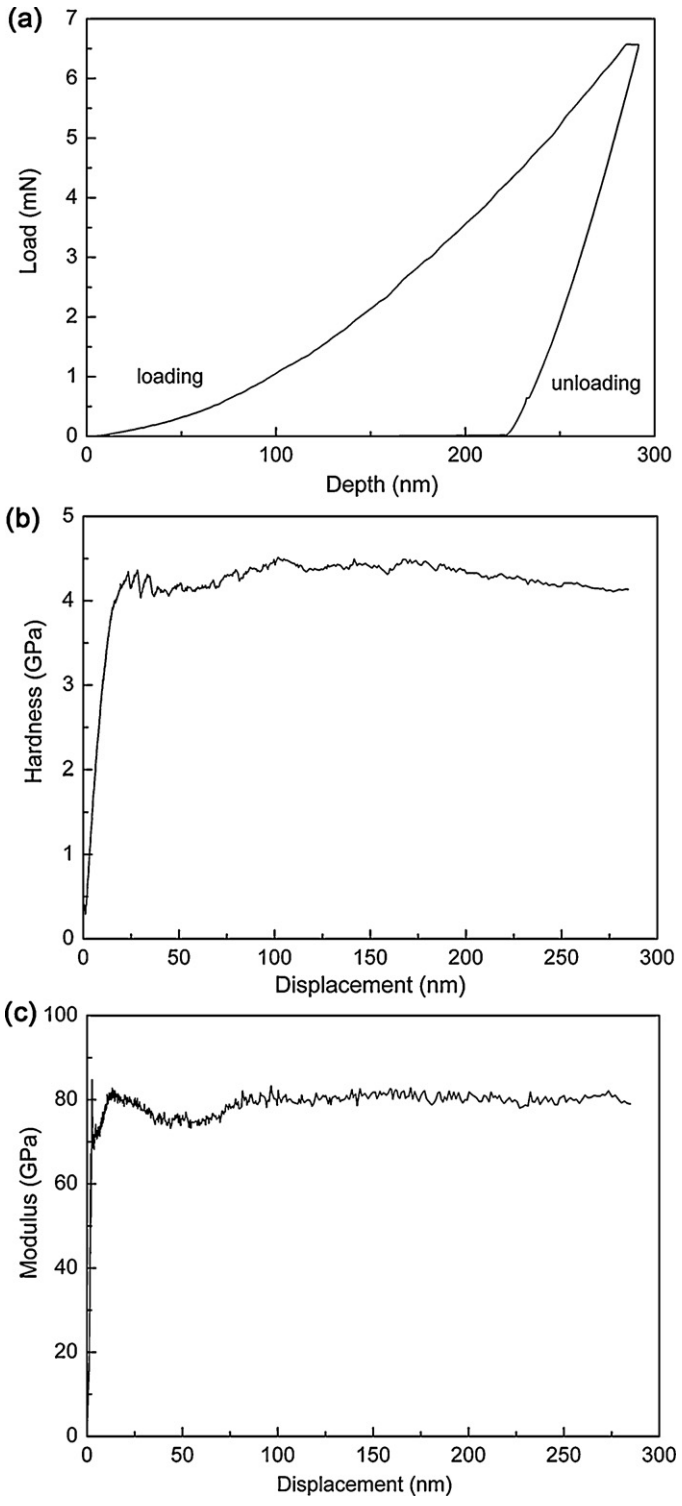

Fig. 4. (a) Loading and unloading curves, (b) hardness-displacement curve, and (c) modulus-displacement curve of the deposit at a strain rate of 0.05 s^{-1}.

Studies have shown that partially crystallized versions of the Al-based alloys offer the promise of even better mechanical properties when suitable mixtures of nano-scale crystalline, quasi-crystalline or amorphous phase exist [22,24,25]. Considering the above microstructure analysis, it can be concluded that the nanocomposite deposit may exhibit good mechanical properties. Vickers hardness test results showed that the values are 400 ± 10 HV, 420 ± 5 HV, and 420 ± 10 HV, respectively for the top, middle and bottom regions, higher than the fully amorphous ribbons exhibiting 340 ± 10 HV. Fig. 4(a) shows the loading and unloading curves (P–h curves) of the alloy samples taken from the middle part of the deposit thickness, where P is load and h is penetration depth. The amorphous matrix nanocomposite exhibits smooth plastic flow, without displaying obvious steps or pop-in/pop-out events. It is suggested by Greer and Walker [26] that evident shear-banding depended on crystallite size in partial devitrified metallic glasses. The shear-band thickness is typically 10–20 nm [27–29], and in contrast, the nano-scale fcc-Al crystallites in the present deposit are 20–50 nm. Therefore, in the present material, the nanocrystalline fcc-Al would disrupt the pattern of shear bands or suppress the appearance of distinct steps in the loading curve [26]. According to Fig. 4(b) and (c), the average elastic modulus and hardness evaluated from the displacement of 25 nm to 300 nm were found to be 80 GPa and 4.13 GPa (~420 HV), respectively. In order to eliminate the detrimental effect of the pores on compressive or tensile mechanical properties, hot extrusion [15,17] at proper temperature is necessary. The more detailed studies including the mechanical properties of the densified deposit under various processing parameters are currently underway.

4. Conclusions

A novel $Al_{86}Si_{0.5}Ni_{4.06}Co_{2.94}Y_6La_{0.5}$ amorphous matrix nanocomposite plate with a rough diameter of 200 mm and a maximum thickness of 12 mm has been prepared by spray-forming. The microstructure gradient is observed, with 91.7 vol.% amorphous phase for the bottom region, 78% for the middle, and 54.3% for the top. The nanoindentation tests reveal its high microhardness of ~420 HV. The microstructure characterization indicates that the improved mechanical properties may be attributed to the homogeneously dispersed nano-scale fcc-Al in the amorphous matrix. This work further proved the feasibility of achieving substantial fraction of amorphous phase for bulk Al-based alloys by spray forming.

Acknowledgements

This research was financially supported by the National Basic Research Program of China (2007CB613900), National Natural Science Foundation of China (nos. 50631010 and 50771006), and the Innovation Foundation of BUAA for PhD Graduates.

References

[1] Y. He, S.J. Poon, G.J. Shiflet, Science 241 (1988) 1640–1642.
[2] A.P. Tsai, A. Inoue, T. Masumoto, Metall. Trans. 19A (I) (1988) 1369–1370.
[3] A. Inoue, Prog. Mater. Sci. 43 (1988) 365–415.
[4] H. Yang, K.Y. Lim, Y. Li, J. Alloys Compd. 489 (2010) 183–187.
[5] L.C. Zhang, M. Calin, M. Branzei, L. Schultz, J. Eckert, J. Mater. Res. 22 (2008) 1145–1155.
[6] T. Zhou, H. Xia, M.B. Yang, Z.M. Zhou, K. Chen, J.J. Hua, Z.H. Chen, J. Alloys Compd. 509 (2011) L145–L149.
[7] P.S. Grant, Prog. Mater. Sci. 39 (4–5) (1995) 497–545.
[8] J.H. Hattel, N.H. Pryds, Acta Mater. 52 (2004) 5275–5288.
[9] F.L. Catto, T. Yonamine, C.S. Kiminami, C.R.M. Afonso, W.J. Botta, C. Bolfarini, J. Alloys Compd. (2010) 026, doi:10.1016/j.jallcom.2011.02.
[10] C.R.M Afonso, C. Bolfarini, C.S. Kiminami, N.D. Bassim, M.J. Kaufman, M.F. Amateau, T.J. Eden, J.M. Galbraith, Scripta Mater. 44 (2001) 1625–1628.
[11] C.R.M. Afonso, C. Bolfarini, C.S. Kiminami, N.D. Bassim, M.J. Kaufman, M.F. Amateau, T.J. Eden, J.M. Galbraith, J. Non-Cryst. Solid 284 (2001) 134–138.
[12] M.L. Ted Guo, Chi Y.A. Tsao, J.C. Huang, J.S.C. Jang, Mater. Sci. Eng. A 404 (2005) 49–56.
[13] M.L. Ted Guo, Chi Y.A. Tsao, J.C. Huang, J.S.C. Jang, Intermetallics 14 (2006) 1069–1074.
[14] A. Garcia-Escorial, M. Echevarria, M. Lieblich, I. Stone, J. Alloys Compd. 504S (I) (2010) S519–S521.
[15] V.C. Srivastava, K.B. Surreddi, S. Scudino, M. Schowalter, V. Uhlenwinkel, A. Schulz, J. Eckert, A. Rosenauer, H.-W. Zoch, Mater. Sci. Eng. A 527 (2010) 2747–2758.

[16] K.P. Lin, ChiY.A. Tsao, J.C. Huang, J.S.C. Jang, Proc. MRS-T, Chinese Society for Materials Science (2009) 336.
[17] T.Y. Dong, B. Yang, J.P. He, Y. Zhang, Acta Metall. Sin. 44 (2008) 659–664.
[18] B.J. Yang, J.H. Yao, J. Zhang, H.W. Yang, J.Q. Wang, E. Ma, Scripta Mater. 61 (2009) 423–426.
[19] L.C. Zhuo, S.J. Pang, H. Wang, T. Zhang, Chin. Phys. Lett. 26 (2009) 066402.
[20] J. Mu, H.M. Fu, Z.W. Zhu, A.M. Wang, H. Li, Z.Q. Hu, H.F. Zhang, Adv. Eng. Mater. 21 (2009) 1–3.
[21] Z. Bian, H. Katoa, C.L. Qin, W. Zhang, A. Inoue, Acta Mater. 53 (2005) 2037–2048.
[22] Y.H. Kim, A. Inoue, T. Masumoto, Mater. Trans. 32 (1991) 559.
[23] S. Annavarapu, R. Doherty, Int. J. Powder Metall. 29 (1993) 331–343.
[24] Z.C. Zhong, X.Y. Jiang, A.L. Greer, Mater. Sci. Eng. A 226–228 (1997) 531–535.
[25] A.R. Yavari, W.J. Botta Filho, C.A.D. Rodrigues, C. Cardoso, R.Z. Valiev, Scripta Mater. 46 (2002) 711–716.
[26] A.L. Greer, I.T. Walker, Mater. Sci. Forum 77 (2002) 386–388.
[27] Y. Zhang, A.L. Greer, Appl. Phys. Lett. 89 (2006) 071907.
[28] P.E. Donovan, W.M. Stobbs, Acta Metall. Mater. 29 (1981) 1419–1436.
[29] A. Castellero, S.J. Lloyd, S.V. Madge, Zs. Kovacs, J.F. Löffler, M. Baricco, A.L. Greer, J. Alloys Compd. 434–435 (2007) 48–51.